Astron. Astrophys. 356, 11–22 (2000)

ASTRONOMY AND ASTROPHYSICS

The enigmatic soft X-ray AGN RX J0134.2–4258⋆

D. Grupe[1], **K.M. Leighly**[2], **H.-C. Thomas**[3], **and S.A. Laurent-Muehleisen**[4]

[1] MPI für Extraterrestrische Physik, Giessenbachstrasse, 85748 Garching, Germany
[2] Columbia Astrophysics Laboratory, 550 West 120th St., New York, NY 10027, USA
[3] MPI für Astrophysik, Karl-Schwarzschild-Strasse 1, 85748 Garching, Germany
[4] UC-Davis and IGPP/LLNL, 7000 East Av., Livermore, CA 94550, USA

Received 8 June 1999 / Accepted 12 January 2000

Abstract. We report the discovery and analysis of the follow-up ROSAT pointed observation, an ASCA observation and optical and radio observations of the enigmatic soft X-ray AGN RX J0134.2–4258. In the optical, RX J0134.2–4258 appears as an extreme 'Narrow-Line Seyfert 1 galaxy' (NLS1), with very strong FeII emission, very blue optical continuum spectrum and almost no Narrow Line Region emission. While its spectrum was one of the softest observed from an AGN during the ROSAT All-Sky Survey, its spectrum was found to be dramatically harder during a pointed observation although the count rate remained constant. We found in the pointed observation that the spectrum is softer when it is fainter and spectral fitting demonstrates that it is the hard component that is variable. The ASCA observation confirms the presence of a hard X-ray power law, the slope of which is rather flat compared with other NLS1s. Survey and followup radio observations reveal that RX J0134.2–4258 is also unusual in that it is a member of the rare class of radio-loud NLS1s, and, with R=71, it holds the current record for largest radio-to-optical ratio in NLS1s. We discuss possible scenarios to explain its strange behaviour.

Key words: acceleration of particles – galaxies: active – galaxies: nuclei – galaxies: quasars: individual: RX J0134.2–4258

1. Introduction

With the launch of the X-ray satellite ROSAT in 1990 (Trümper 1983) a new window was opened for astronomy. One of ROSAT's first tasks was to perform the first all-sky survey in the 0.1-2.4 keV energy band, the ROSAT All-Sky Survey (RASS; Voges 1993; Voges et al. 1999). A large number of Active Galactic Nuclei (AGN) with extremely steep X-ray spectra were discovered in this survey (e.g. Thomas et al. 1998; Grupe et al. 1998a, 1999; Beuermann et al. 1999). Some soft X-ray AGN appear to be transient in the ROSAT Position Sensitive Proportional Counter energy window (PSPC, Pfeffermann et al. 1986). These AGN were bright only in their 'high' state during the RASS. Some prominent examples are IC 3599 (Brandt et al. 1995; Grupe et al. 1995a), WPVS007 (Grupe et al. 1995b), and NGC 5905 (Bade et al. 1996; Komossa & Bade 1999). Both IC 3599 and NGC 5095 showed a similar decrease by about a factor 70 which suggests that they were experiencing an X-ray outburst during the RASS. WPVS007 showed a decrease by a factor of $\sim$ 400 between the RASS and a pointed observation about three years later, and was practically turned off after that. The situation in RX J0134.2–4258 appears to be different. While its count rate remained nearly constant between the RASS and the pointed PSPC observation about two years later, its spectral shape changed dramatically. Together with WPVS007, it had the steepest soft X-ray spectrum during the RASS, but in the pointed observation it showed a flat spectrum (Mannheim et al. 1996). Follow-up medium resolution spectroscopy showed this object to be a Narrow-Line Seyfert 1 galaxy with a blue optical spectrum and very strong FeII emission. It is one of the most peculiar sources in our sample of bright soft X-ray selected ROSAT AGN (see Grupe et al. 1998a, 1999).

In Sect. 2 we describe the observations and data reduction. Sect. 3 gives a summary of the results of the ROSAT, ASCA and optical observations, and in Sect. 4 we discuss possible scenarios that may explain the strange behaviour found in this object.

2. Observations and data reduction

RX J0134.2–4258 was observed during the RASS between 1990, December 09, 20:42h and 1990, December 17, 23:11h for a total of 574 s. Photons were collected in a circle of 250" in radius for the source and two circles of 400" in the scan direction for the background.

About two years after the RASS observation, RX J0134.2–4258 was observed again by ROSAT between 1992, December 28, 19:08h and 1993, January 03, 23:37h, for a total of 7467 s. The same size extraction regions were used, with the background taken from a source-free area near RX J0134.2–4258. The pointed observation count rate was measured in channels 11-201, and spectral fitting was performed over the same band. All power law model index values are quoted in terms of the energy spectral index $\alpha_{\rm X}$ with $\rm F_\nu \propto \nu^{-\alpha}$. The hardness ra-

Send offprint requests to: D. Grupe (dgrupe@xray.mpe.mpg.de)

⋆ Based in part on observations at the European Southern Observatory La Silla (Chile) with the 2.2m telescope of the Max-Planck-Society during MPG and ESO time, and with the ESO 1.5m telescope in September/October 1995

Table 1. X-ray, optical, and radio positions of RX J0134.2–4258. "2σ" marks the 2σ error radius, and Δ markes the distances of the radio and X-ray positions to the optical position, all given in arcsec

Observation	α_{2000}	δ_{2000}	$\alpha\ 2\sigma$	$\delta\ 2\sigma$	Δ
RASS	01 34 16.9	–42 58 08	20.0	20.0	20
Pointed Obs.	01 34 16.7	–42 58 28	2.0	2.0	2
Optical(USNO)	01 34 16.9	–42 58 27	0.5	0.5	0.0
Radio (PMN 4.85 GHz)	01 34 10.6	–42 58 49	48	40	55
Radio (VLA 8.4 GHz)	01 34 16.9	–42 58 22	1.7	14	5

tio was defined by $HR = \frac{hard-soft}{hard+soft}$, where the soft and hard bands correspond to channels 11-41 and 52-201, respectively. RX J0134.2–4258 was also observed with the ROSAT High Resolution Imager (HRI) between 1996, June 17, 01:57h and 03:22h (UT) for a total of 2393 s.

Our ASCA (Tanaka et al. 1994) observation was performed on 1997 December 10. Standard methods using FTOOLS 4.1 were used to reduce the data. The net exposures were 45.6, 45.8, 51.0, 51.0 ks for SIS0, SIS1, Gas Imaging Spectrometer (GIS) 2 and GIS3, respectively.

Optical spectra were obtained at different times. The first low-resolution spectrum was obtained in August 1993 with the 2.2m MPG/ESO telescope in La Silla. A medium resolution spectrum taken about a month later under photometric conditions at the same telescope is presented in Grupe et al. (1999). The spectrum we present in this paper, which has the best signal to noise, was taken in four nights in September/October 1995 using the Boller & Chivens spectrograph at the ESO 1.5m telescope with grating #23 which has 600 grooves mm^{-1} and a dispersion of 126 Å mm^{-1} in first order. The spectral resolution was $\sim$ 5Å. The camera was equipped with a FA 2048L 2048×2048 CCD with a pixel size of $15{\times}15\mu\mathrm{m}^2$ (ESO CCD #24). The total observing time was 3.25 hours. The conditions were cloudy and therefore the absolute flux cannot be measured from this spectrum. We measure $\mathrm{m_V} = 16.0$ from the spectrum obtained under photometric conditions (Grupe et al. 1999). RX J0134.2–4258 was also observed by the HST (Goodrich 2000) From this spectrum $\mathrm{m_V} = 16.2$ was measured.

A radio source was detected in the Parkes-MIT-NRAO (PMN) Surveys near the position of RX J0134.2–4258 (Wright et al. 1994). In order to obtain a better radio position, on May 7 1999 we observed RX J0134.2–4258 at 8.4 GHz while the VLA[1] was in the D-configuration. Time on source was approximately 36 min. Absolute flux calibration was set by a short observation of 3C 286 and another calibrator close in position to RX J0134.2–4258 was observed to correct the phases. Data were calibrated and reduced in the standard iterative manner using the NRAO's AIPS analysis package (v15APR98) and using the tasks MX and CALIB. Self-calibration for correction of only the phases was applied in order to preserve the absolute flux density scale. The noise in the final map is 0.18 mJy and because of the very low declination of this source, the beam is an elongated $41.6'' \times 5.2''$ at an PA of $\approx 0°$. The source is completely unresolved in our map.

[1] The VLA and NRAO are operated by Associated Universities, Inc., under cooperative agreement with the National Science Foundation.

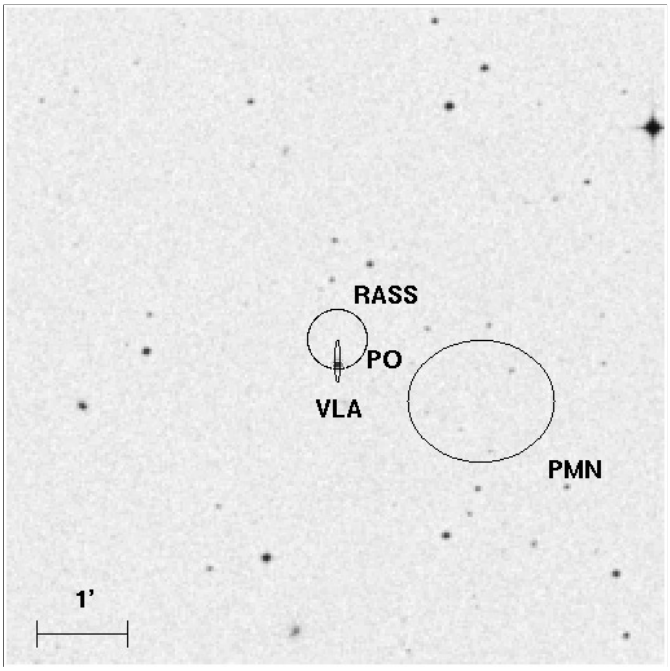

Fig. 1. Finding chart of RX J0134.2–4258. The circles/ellipes mark the 2σ error of the RASS, the ROSAT pointed observations (PO), the PMN radio survey, and the VLA observation. See text for details. The ROSAT pointed observation error circle fell directly on the source.

3. Results

Fig. 1 shows the $7' \times 7'$ finding chart of RX J0134.2–4258 and the measured X-ray, optical, and radio positions of RX J0134.2–4258 are given in Table 1. The 2σ (90% confidence) error circles of the RASS and pointed observations are marked. The optical position was derived from the US Naval Observatory scans of the ESO/SRC plates. The X-ray source corresponds to an optical counterpart that was identified as an AGN at z=0.237 (Grupe et al. 1998a). The error circle of the RASS observation was estimated by fitting a Gaussian profile to the data and averaging the positional uncertainties in RA and DEC. The position and error circle of the pointed observation was determined by using a maximum likelihood algorithm in the EXSAS software package (Zimmermann et al. 1998).

The 4.85 GHz radio position was obtained in the Parkes-MIT-NRAO (PMN) radio survey (Wright et al. 1994). The uncertainty on this position, which depends on the location and flux of the object (see Wright et al. 1994 for details), indicate that the optical position of RX J0134.2–4258 is nearly 3σ in RA from the cataloged radio source (Fig. 1). This fact, casting significant doubt on the possibility that the optical and radio sources were associated, prompted us to make a new pointed observation using the VLA. We used the task JMFIT on the new VLA data to fit a gaussian to the peak of the emission. The position and uncertainty (taken to be 1/3 the beam in each

Table 2. Spectral fits to the RASS and pointed observation X-ray data of RX J0134.2–4258. "$N_{\rm H}$" is the column density given in units of $10^{20}{\rm cm}^{-2}$, "Norm" is the normalization at 250 eV (rest frame) in 10^{-3} Photons cm^{-2} s^{-1} keV^{-1}, "$\alpha_{\rm X-soft}$" the soft energy spectral slope, "Break" the break energy in keV of the broken power law fit (rest frame), "$\alpha_{\rm X-hard}$" the hard energy spectral slope, "A" the black body integral in Photons cm^{-2} s^{-1}, and "$T_{\rm rad}$" the radiation temperature in eV. The models used here are simple power laws (powl), broken power laws (brpl), Black body (bbdy), and a black body plus power law (bbpl).

Observation	model	$N_{\rm H}$	Norm	$\alpha_{\rm X-soft}$	Break	$\alpha_{\rm X-hard}$	A	$T_{\rm rad}$	χ^2/ν
RASS	powl	0.27±1.11	7.20±1.95	2.68±5.63	—	—	—	—	1.5/5
RASS	powl	1.59 fix	6.04±4.97	6.94±2.60	—	—	—	—	2.2/5
RASS	bbdy	1.59 fix	—	—	—	—	0.63±1.45	24±8	2.5/4
RASS	bbpl	1.59 fix	0.43±1.44	—	—	1.00 fix	0.72±0.15	23 fix	2.3/6
Pointed	powl	0.61±0.37	5.49±1.57	0.80±0.07	—	—	—	—	43/40
Pointed	powl	1.59 fix	10.20±0.56	1.22±0.06	—	—	—	—	58/41
Pointed	brpl	1.59 fix	12.90±10.50	6.17±5.00	0.27±0.02	1.00 fix	—	—	40/40
Pointed	brpl	1.59 fix	17.11±1.40	3.83±1.46	0.34±0.05	0.80 fix	—	—	44/40
Pointed	bbdy	1.59 fix	—	—	—	—	0.004±0.0003	145±4	349/41
Pointed	bbpl	1.59 fix	10.0±9.5	—	—	1.04±1.22	8.75±0.01	14±7	40/39
Pointed	bbpl	1.59 fix	14.6±3.3	—	—	1.00 fix	0.15±0.03	23 fix	42/41
OBI 3	bbpl	1.59 fix	2.25±1.58	—	—	1.00 fix	0.20±0.89	23±3	8.5/8
OBI 5	bbpl	1.59 fix	15.3±17.6	—	—	1.00 fix	0.12±1.5	23±32	7.3/11

direction) are shown on Fig. 1 and listed in Table 1. We assert that the coincidence of the radio source and RX J0134.2–4258 is such to warrant a confident association of the optical/X-ray source with this radio object.

3.1. ROSAT

The RASS observation yielded 120±29 counts, giving a count rate of 0.21±0.05 cts s^{-1} and an HR of −0.84±0.05 (Grupe et al. 1998a, 1999). A power law plus absorption model reveals that the intrinsic absorption in this source appears to be negligible and therefore the absorption was fixed at the Galactic value ($N_{\rm H}$ = 1.59 10^{20} cm^{-2}; Dickey & Lockman 1990). The resulting energy spectral index is very steep: $\alpha_{\rm x}$ =6.9±2.9. Spectral fitting results are given in Table 2, and the result of this fit is shown in Fig. 2. A blackbody model was also fitted. The absorption column density approached zero when it was allowed to be free and therefore it was again fixed at the Galactic value. The resulting radiation temperature was 24±8 eV. We cannot distinguish between a power law and a black body model for the RASS data. The low signal to noise of the spectrum did not allow more sophisticated fits.

The pointed ROSAT PSPC observation yielded 1476±43 counts corresponding to a count rate of 0.20±0.01 cts s^{-1}. This was nearly the same rate as was found in the RASS observation; however, the spectrum was much harder (HR=−0.12±0.01). A single power law fit to the total pointed observation spectrum with column density fixed to the Galactic value does not give a satisfactory description of the soft spectrum (Fig. 3, left panel). A single black body model does not give a good fit either. A broken power law gave a much better fit (Fig. 3, middle panel). However, to determine the uncertainties on the model parameters, it was necessary to fix the slope of the hard power law. We used two values: $\alpha_{\rm x}$=1.0, the result of the free fit, and $\alpha_{\rm x}$=0.8, the result from the ASCA spectra (see Sect. 3.2). Interestingly, for

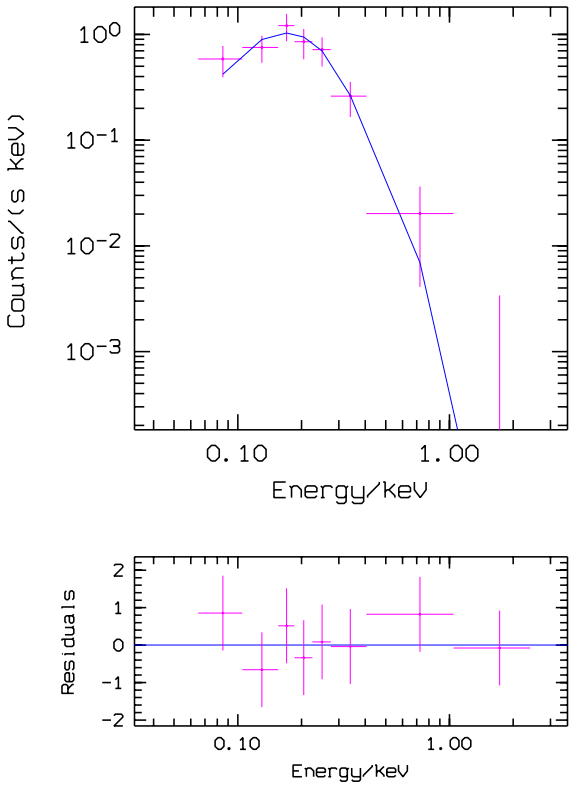

Fig. 2. Power law fit to the RASS spectrum of RX J0134.2–4258. The cold absorption parameter was fixed to the Galactic value. The X-ray spectral slope is $\alpha_{\rm x}$ = 6.9±2.9.

both cases, we found that the soft X-ray component had a similar slope as was found during the RASS observation. A black body plus a power law also fit the spectrum well (Fig. 3, right panel); in this case, all parameters except for the absorption, which was still fixed to the Galactic value, could be left free. These spectral fitting results are also summarized in Table 2.

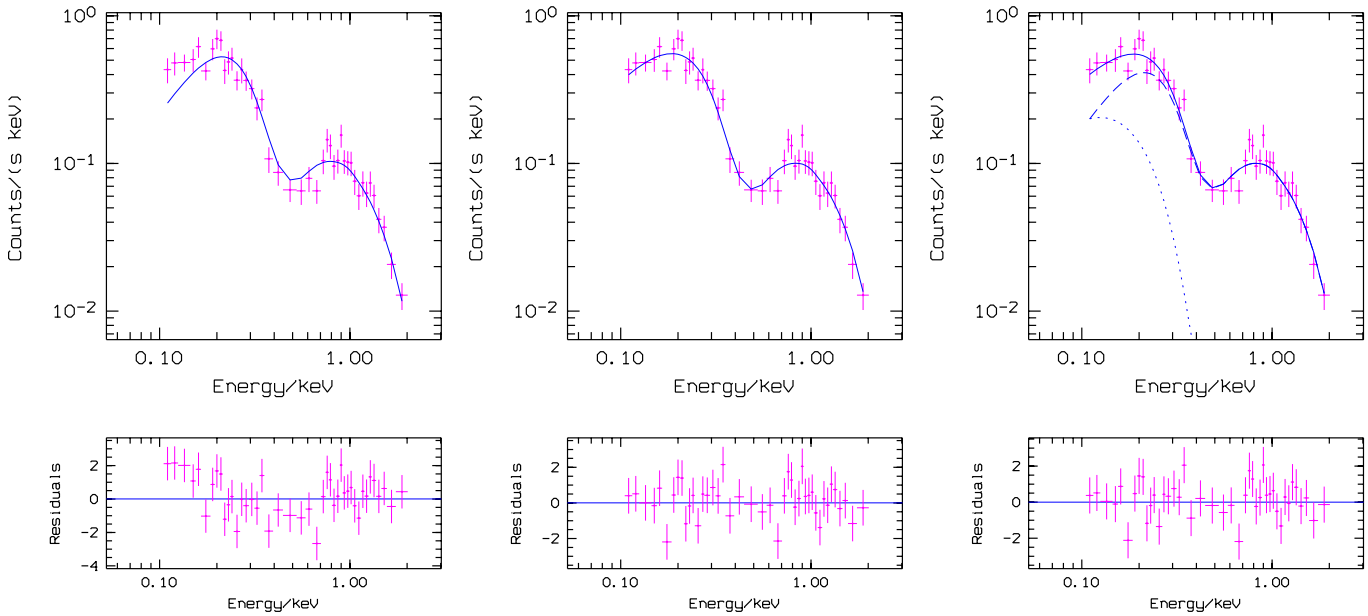

Fig. 3. Spectral fits to the pointed observation spectrum of RX J0134.2–4258: a single power law fit (left panel), with $N_{\rm H}$ fixed to the Galactic value; a broken power law fit(middle panel), also fixed $N_{\rm H}$ and the high energy power law slope fixed to $\alpha_{\rm x}$=1.0; and an absorbed black body plus power law spectral fit (right panel). The fit parameters are given in Table 2.

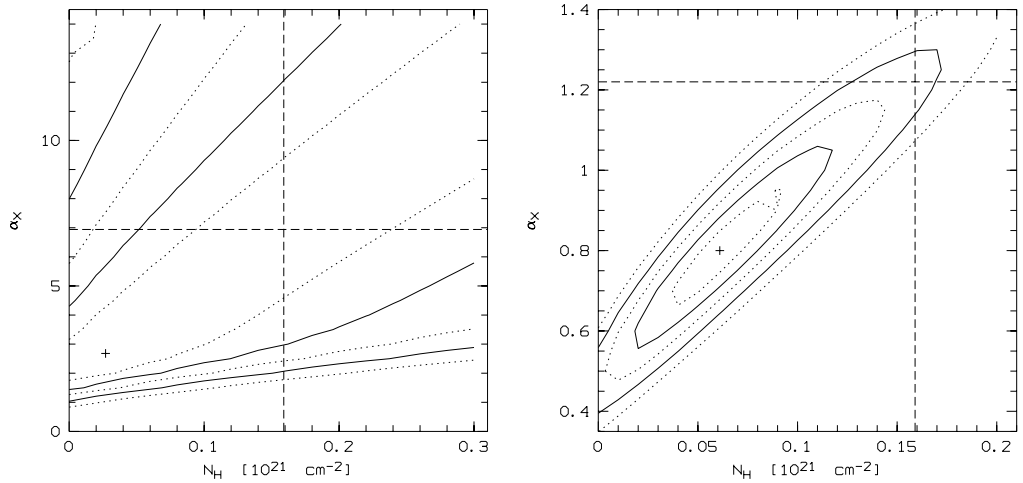

Fig. 4. Contour plots of power law fits to the X-ray data. The left panel shows the RASS data and the right one the pointed observation. The dashed straight lines mark the results of a fit with fixed column density ($N_{\rm H}$ =0.159). The contours are at 1, 2, 3, 4, and 5 σ level.

We can infer the presence of a soft excess if a power law plus absorption model yields a column density less than the Galactic value. Fig. 4 displays the contours of power law fits to the RASS and pointed observation spectra with the absorption column free. The RASS spectra are consistent with a single power law model; however, the measured column density for the pointed observation is less than the Galactic column density, indicating the presence of a soft excess.

No significant variability was detected from the RASS light curve; however, the statistics are poor enough that we cannot exclude variability with high confidence. The pointed observation consisted of 6 observation intervals (OBI); each OBI corresponds roughly to a 1 or 2 orbit exposure. Binning the data in each OBI showed clear variability in both the flux and hardness ratio (Fig. 5). The spectral variability is correlated with the flux variability in that the spectrum becomes *harder* when the count rate *increases*. Fig. 6 displays how the spectra changed. While the soft channels remain practically constant, the hard channels became fainter by a factor of almost 10. To investigate this further, we made spectral fits of OBIs 3 and 5 using a two component spectral model consisting of an absorbed black body and a power law (Table 2). These fits show that the radiation temperature of the spectra remains the same, and the biggest variation is seen in the normalization of the power law component. This means that the spectral variability can be consistently explained as originating from variability in the flux of the hard component.

RX J0134.2–4258 was not detected during the ROSAT HRI observation. An upper limit of 0.0011 cts $\rm s^{-1}$ was measured. Assuming the power law fit to the OBI 3 data, a count rate of 0.0028 cts $\rm s^{-1}$ was expected. We infer that during the one and a half hours of the observation the hard X-ray component was in

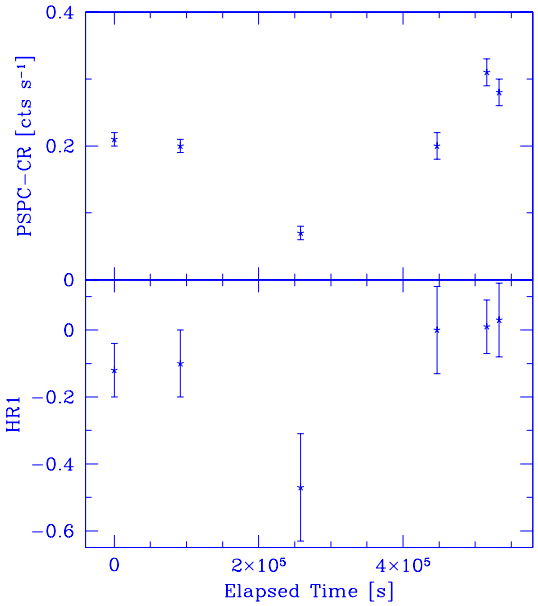

Fig. 5. Light curve of RX J01334.2–4258 during the pointed observation between 92/12/28 and 93/01/03 (OBIs 1-6). The start time is 92/12/28 19:08 (UT). The upper panel shows the change in the count rate and the lower one the spectral behaviour in the hardness ratio 1.

Table 3. X-ray positions of the sources surrounding RX J0134.2–4258. The source number corresponds to the marked positions in Fig. 7.

Source	α_{2000}	δ_{2000}
#1	01 33 20.5	–43 04 31.5
#2	01 34 04.5	–42 51 34.7
#3	01 34 01.9	–42 56 38.2
#4	01 34 12.7	–43 01 34.8

its low state. The HRI is much less sensitive to lower energies than the PSPC; therefore the soft X-ray component was not detected.

3.2. ASCA

RX J0134.2–4258 was clearly detected in our ASCA images. Fig. 8 shows the smoothed, combined GIS2 and GIS3 ASCA image in the hard (2.0–5.0 keV) band; RX J0134.2–4258 is the brightest source in the field, but several other sources are visible. The superior Point Spread Function (PSF) available from the *ROSAT* PSPC allowed us to identify several nearby X-ray emitting sources that could contaminate the ASCA spectrum (Fig. 7) and their positions are listed in Table 3. None of these objects have catalogued identifications.

The nominal source extraction regions, with radii 4 and 6 arcminutes for the SIS and GIS respectively, were used initially. The background spectra were estimated using source-free regions of the detectors. The source was not detected at high energies and thus the spectra were fitted in the energy bands 0.5–7.0 and 0.8–8.0 keV for the SIS and GIS respectively. The net count rates were 0.017, 0.016, 0.010 and 0.013 cts s^{-1} in SIS0, SIS1, GIS2 and GIS3, respectively. We fitted all four spectra separately, and found that, as usual, SIS1 yielded slightly flatter spectral parameters and higher absorption. However, the four detectors were consistent within 90% confidence and therefore all data from all detectors were used for spectral fitting.

Spectral fitting revealed evidence that the ASCA spectrum is contaminated by a nearby source. For the source extraction regions listed above, the GIS flux is about 40% larger than that of the SIS. While the cross calibration between detectors is not perfect, the differences should not be more than about 10%

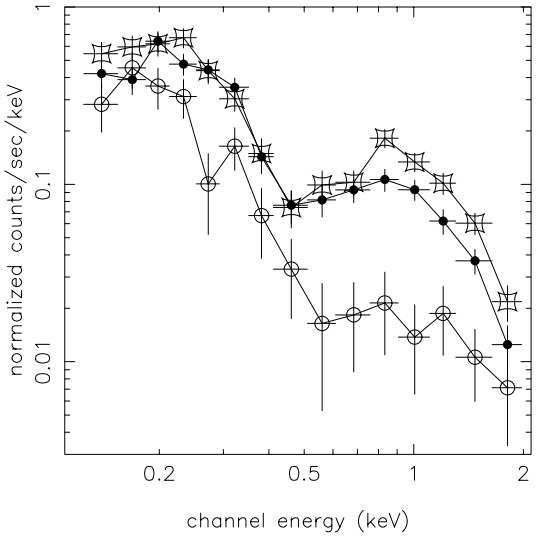

Fig. 6. Spectra of the ROSAT pointed observation. The solid circle are OBIs 1 and 2, the open circles are OBI 3, and the squares are OBIs 4-6.

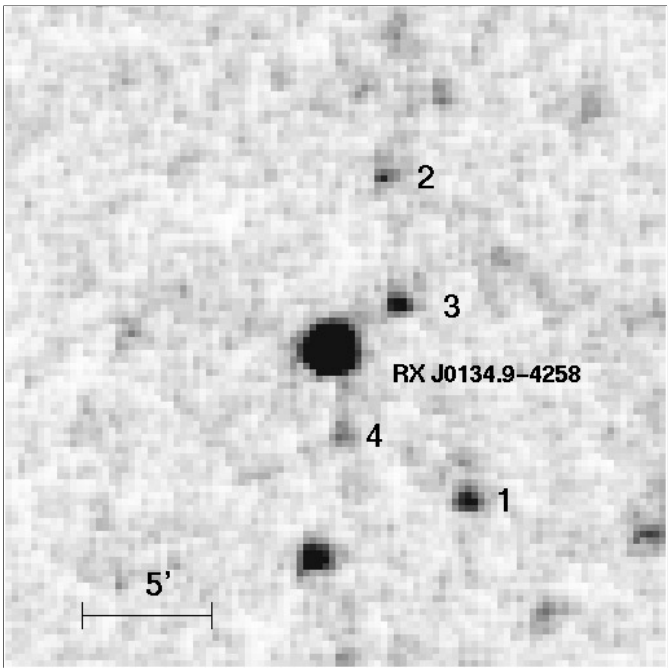

Fig. 7. ROSAT PSPC image from the pointed observation of RX J0134.2–4258. The positions of the surrounding sources 1 - 4 are given in Table 3.

Table 4. Spectral analysis of the ASCA observation plus the combined ASCA + ROSAT spectral fit (below)

Parameter	All[1]	SIS only	2' extr. reg.[2]
$\alpha_{\rm X}$	$0.78^{+0.1}_{-0.09}$	0.77±0.12	0.85±0.09
Flux SIS0	4.8	4.7	4.0
Flux SIS1 (2-10 keV)	4.8	4.8	4.2
Flux GIS2	6.6	—	4.5
Flux GIS3	7.3	—	4.5
$\alpha_{\rm X}$ above 2keV	$0.62^{+0.26}_{-0.25}$	$0.4^{+0.9}_{-0.4}$	$0.78^{+0.30}_{-0.29}$
Fe flux limit	<2.3	<4.7	<1.8
Fe eqw limit (eV)	<260	<550	<250
0.74 keV edge depth	<0.61	<0.74	$0.83^{+0.53}_{-0.64}$
0.87 keV edge depth	<0.43	<0.46	<0.30
Intrinsic abs (10^{20})	<0.4	<0.5	<1.4

[1] SIS, GIS extraction regions 4 and 6 arcmin; may include contaminating source.
[2] SIS, GIS extraction regions 2 arcmin

Parameter	ASCA + ROSAT fit
$\alpha_{\rm X}$	0.80±0.09
kT (eV)	30^{+15}_{-9}
2–10 KeV flux (SIS0)[1]	4.58
2–10 keV luminosity[2]	1.32
0.1–2.0 keV flux[1]	14.0
0.1–2.0 keV luminosity[2]	3.8
neutral absorption	$< 2.0\ 10^{20}{\rm cm}^{-2}$
τ (0.74 keV)	< 0.33
τ (0.87 keV)	< 0.27
Fe K line flux[3]	< 2.5
Fe K equivalent width	< 295

(Notes: confidence intervals are 90% for one parameter of interest; i.e. $\Delta\chi^2 = 2.71$.)
([1] continuum fluxes are in 10^{-16} W m^{-2},
[2] Luminosities in 10^{37} W,
[3] Fe line flux in 10^{-6} photons cm^{-2} s^{-1})

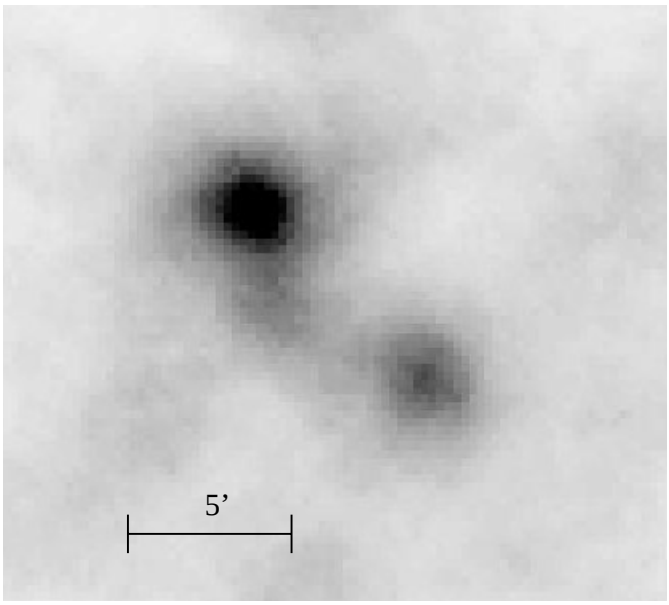

Fig. 8. ASCA 2-5 keV GIS image of RX J0134.2–4258, the brightest source in the image. The weak source about 3.5' south of RX J0134.2–4258 corresponds to source #4 in Fig. 7 and the other brighter source about 7' southwest of RX J0134.2–4258 corresponds to source #1.

(this number is not known exactly because of changes in the SIS efficiency). The suspected contaminating source is #4 for the following reasons. First, it is about $3.5'$ from RX J0134.2–4258, and therefore it falls within the $6'$ GIS extraction region. Also, it can be seen as a faint extension toward the south in the ASCA image (Fig. 8); in contrast, source #3, which is also about $3.25'$ from RX J0134.2–4258, is not clearly present in the ASCA image. Thirdly, the difference in fluxes between SIS and GIS increases as the source extraction region sizes are increased. This is expected because the GIS has a broader point spread function, but more importantly because the position of this contaminating source means that it falls off the chip completely for SIS1 and partially for SIS0. The photon index from a power law fit to all four detectors increases slightly as the source extraction region is decreased. This result suggests that the contaminating source may be somewhat harder than RX J0134.2–4258. This source is less than 6% as bright as RX J0134.2–4258 in the pointed ROSAT observation; however, the flux measurements listed above suggest that it contributes more than $\sim 20\%$ to the ASCA spectrum. The difference may be due to a harder spectrum for the contaminating source (although analysis of the ROSAT spectrum does not clearly indicate this) or variability. A faint (magnitude ~ 19) counterpart is visible in the DSS image at the X-ray position; however, there is no cataloged identification. Because of the possible contamination, we list spectral fitting results from the regions listed above, as well as SIS alone and SIS+GIS with extraction regions $2'$ in radius at which the contamination by a source $3.5'$ distant should be minimal.

3.2.1. ASCA spectral fitting results

The spectra were first fitted with a power law plus Galactic absorption, and a good fit was obtained (Fig. 9). No features are apparent in the spectra. Iron lines are frequently found in the ASCA spectra of Seyfert galaxies, although there appears to be some dependence on luminosity (e.g. Nandra et al. 1997). Addition of a narrow ($\sigma = 50\,{\rm eV}$) iron line does not improve the fit; the upper limit is given in Table 4. Because the upper limit on the equivalent width is consistent with those measured from iron lines detected in other Seyfert galaxies as luminous as RX J0134.2–4258 (1.4×10^{37} W corresponding to a 2–10 keV flux of 4.8×10^{-16} W m^{-2}) we conclude that the statistics are too poor to recognize the iron line if present. Evidence for ionized or "warm" absorption is also frequently found in the ASCA spectra of Seyfert galaxies (e.g. Reynolds 1997). Addition of absorption edges at 0.74 and 0.87 keV in the rest frame, relevant for absorption by O VII and O VIII respectively, did not improve the fit significantly, except in the case where the extraction region was $2'$ ($\Delta\chi^2 = 5.1$ for 1 degree of freedom). However, the observed energy of this edge for z=0.237 is 0.6 keV, very

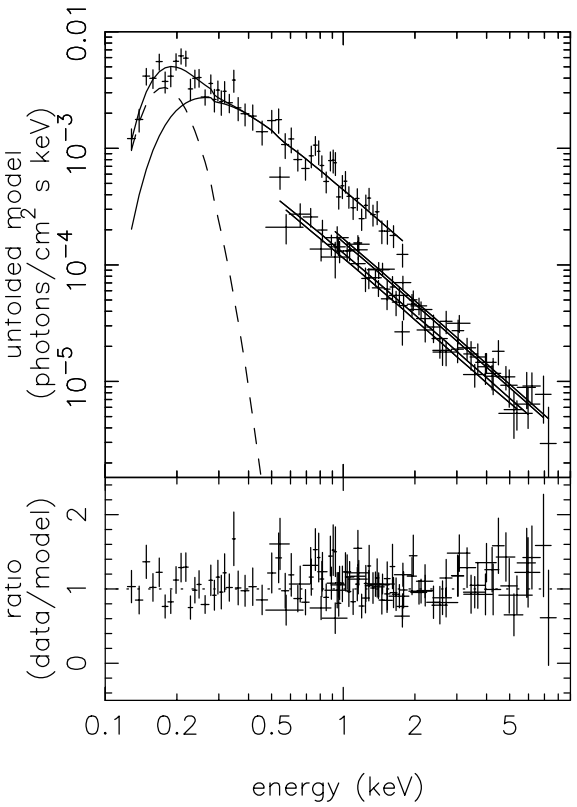

Fig. 9. Combined power law + blackbody fit to the ROSAT and ASCA spectra.

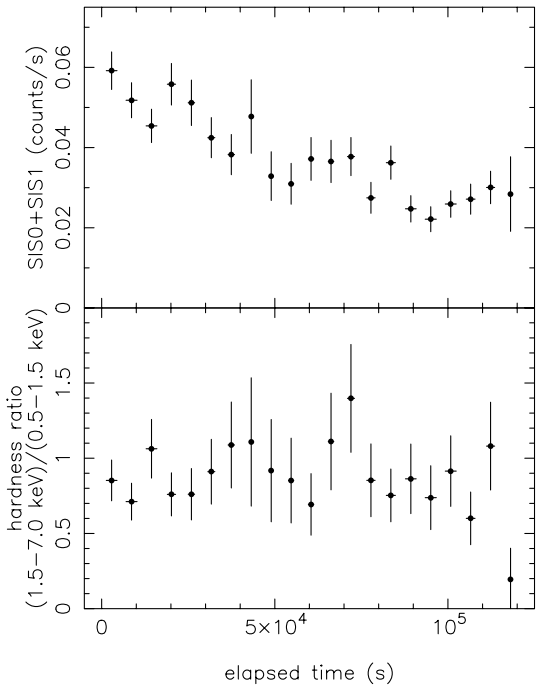

Fig. 10. The ASCA light curve. The upper panel shows the count rate variation. The lower panel, showing the hardness ration as a function of time, indicates that no significant spectral variability was detected.

near the edge of the bandpass in the SIS in the observer's frame. Since it is not detected with the other extraction regions, the reality of this feature is suspect. The upper limits (Table 4) encompass typical optical depths found in Seyferts and NLS1s (e.g. Leighly 1999a) and we conclude that the poor statistics prevent detection of a typical warm absorber. However, a warm absorber with very large optical depth ($\tau > 1$) is clearly ruled out.

The power law energy spectral index in RX J0134.2–4258, measured to be 0.8, has the distinction of being rather flat for an NLS1. In a study of 25 spectra from 23 NLS1s, Leighly (1999a) found an average index $\alpha_{\rm x}$ of 1.19 with an intrinsic dispersion of 0.3. Therefore, such a flat index is not unknown. However, the other cases of best fit indices $\alpha_{\rm x} < 1.0$ occurred in Mrk 766 and NGC 4051, both of which have somewhat peculiar properties for NLS1s, or in objects with complex spectra and very weak hard tails (PHL 1092, PG 1404+226, and Mrk 507). Steeper hard spectra were found in other objects. Leighly (1999a) also found that many NLS1s that have little evidence for absorption have evidence for a soft excess. There is a little evidence for a weak soft excess in RX J0134.2–4258 in that that best fit value above spectral slope above 2 keV, measured to be 0.6, is flatter than the best fit index over the whole energy band. However, the indices are consistent within their statistical error, and addition of a soft excess component does not improve the fit significantly. It is interesting to note, for reasons that will become apparent below, that the spectral index is quite close to the average found from radio-loud quasars observed by GINGA (0.72 ± 0.07; Lawson & Turner 1997).

Because it appears that the ROSAT and ASCA spectral fitting results may be consistent except for a normalization factor arising from variability between the two observations, we proceed to make a joint fit (Fig. 9, Table 4). A power law with Galactic absorption provides an acceptable but not a good fit ($\chi^2 = 309$ for 245 d.o.f.) and there are residuals at low and high energies. Addition of a black body improves the fit greatly ($\Delta\chi^2 = 43$ for two additional degrees of freedom). This joint fit shows that the power law component normalization is a factor of about 3.5 larger in the ROSAT pointed observation than in the ASCA observation. Again, no additional absorption, warm absorber as modeled by O VII and O VIII edges or iron line are required. It has to be noted that in one simultaneous ROSAT and ASCA observation of NGC 5548, ROSAT data systematically appear steeper than ASCA data (Iwasawa et al. 1999) and therefore there is some doubt whether the cross calibration between the two missions is good enough to warrant a simultaneous fit. However, in this case, we see no evidence for a cross calibration problem.

3.2.2. X-ray variability during ASCA observation

We observed RX J0134.2–4258 to vary during the observation. The light curve from the SIS detectors binned by orbit is shown in Fig. 10; a steady decline by a factor of about 2 was observed. We calculated the fractional amplitude of variability, also called the excess variance, defined as the measured variance minus the measurement error and normalized by the square of the mean

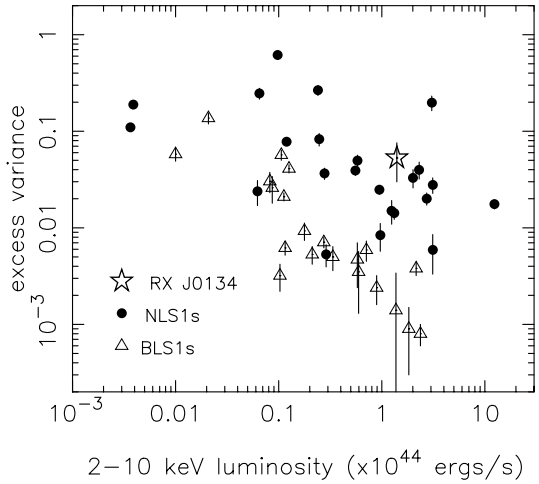

Fig. 11. Excess variance as function of X-ray luminosity. RX J0134.2–4258 has similar excess variance as other NLS1s. (figure adapted from Leighly 1999b).

(e.g. Nandra et al. 1997; Leighly, 1999b). This parameter is a useful one to quantify variability in ASCA observations because it can be shown that under a set of justifiable assumptions, it is related to the inverse of the variability time scale (Leighly 1999b). For a light curve with 128 second binning, the excess variance is 0.053 ± 0.023. Fig. 11, adapted from Leighly (1999b), shows that this excess variance is high compared with broad-line Seyfert galaxies with similar luminosities but consistent with Narrow-line Seyfert 1 galaxies. Therefore, although the hard X-ray spectrum appears to be rather flat for an NLS1, the variability properties are unremarkable.

3.3. Optical

Fig. 12 displays the optical spectrum of RX J0134.2–4258 obtained in September/October 1995. The spectrum is characteristic of a typical Narrow-line Seyfert 1 galaxy. The broad permitted blend of FeII emission commonly present in NLS1s severely contaminates the spectrum, making an accurate measurement of the flux and width, in particular of the Hβ and O[III] lines difficult. In order to account for this, we employ the FeII subtraction method introduced by Boroson & Green (1992) and now commonly used (e.g. Grupe et al. 1999; Leighly 1999a). The FeII emission line spectrum from a high signal-to-noise optical spectrum of the prototype strong Fe emitter I Zw 1 is first convolved with a Gaussian and then scaled until the width and intensity of the lines approximately match those seen in the RX J0134.2–4258 spectrum. This best-fitting FeII model was then subtracted and the remaining emission lines examined.

We measured line widths of FWHM=900$\pm$100 and 670$\pm$200 km s^{-1} for Hβ and [OIII]λ5007, respectively. The ratio of the FeII to Hβ emission is the strongest among all objects in the entire sample of soft X-ray selected AGN ($\frac{\rm FeII}{\rm H\beta}$ = 12.3, see Grupe at al. 1999). As we noted in Grupe et al. 1998a, the object has a very blue spectrum ($\alpha_{\rm opt}$ = –0.1). We were not able to detect any [OIII]λ5007 emission in the spectra taken two years earlier; however, the [OIII] is apparent in the better signal-to-noise spectrum presented here (after FeII subtraction). Otherwise, the results are the same as obtained from our other spectra (Grupe et al. 1999).

3.4. Radio

RX J0134.2–4258 was detected in the Parkes-MIT-NRAO (PMN) survey (Wright et al. 1994) with a flux density of 55$\pm$9 mJy at 4.85 GHz. Our new VLA observation yielded a flux of 25 ± 1.5 mJy at 8.4 GHz and the source is completely unresolved in our map. The two radio fluxes allow us to derive a radio spectral index of -1.4, assuming no variability between the two observations. This radio spectral index is fairly steep compared to core-dominated sources, but not unheard of. Applying the criterion of Kellermann et al. (1989), who use R=10 as the dividing line between radio-loud and radio-quiet quasars[2], the source is radio-loud, since R=71. The radio flux corresponds to a luminosity of log (P) = 25.3 W Hz^{-1}. Thus, also using the luminosity criteria (e.g. Joly 1991; Miller et al. 1993), RX J0134.2–4258 should be classified as a radio-loud AGN. We note, however, that if the steep spectrum is real and not a consequence of variability, the radio flux is highly frequency dependent.

Narrow-line Seyfert 1 galaxies are generally considered to be weak radio sources. Ulvestad et al. (1995) found that the luminosities among 15 NLS1s observed with the VLA were were generally less than log P=22.5 W Hz^{-1}. Only two other NLS1s are known to be radio-loud. One is PKS 0558-504 (e.g. Remillard et al. 1991) and the other is RGB J0044+193 (Siebert et al. 1999). Both of these objects are fairly faint radio sources, with R $\approx$ 31 and 27, respectively. Thus, RX J0134.2–4258 has the relatively strongest radio emission of an NLS1 so far discovered.

It is possible that RX J0134.2–4258 is a variable radio source. It is not a catalogued member of the Parkes 2700 MHz survey catalog. The flux limit of this catalog depends on the location in the sky, but we note that there are catalogued objects within 10 degrees with fluxes as low as 50 mJy, although this appears to be the lower limit of the catalog. The PMN flux at 4.85 GHz predicts a flux of 125 mJy at 2700 MHz, assuming $\alpha = -1.4$; therefore, it should have been detected by the Parkes survey unless it is variable. Objects with steep spectra are generally not variable, but since the observations defining the index were not simultaneous, the steep index could in fact be a consequence of variability. Evidence for variability in the radio has also been found in one of the other radio-loud NLS1s, RGB J0044+193 (Siebert et al. 1999). On the other hand, many NLS1s observed simultaneously at more than one radio frequency show steep rather than flat spectra (Moran et al. in prep.).

3.5. Spectral energy distribution

Fig. 13 displays the spectral energy distribution of our source. The object was also detected by IRAS at 60 μm and we display

[2] R is defined as the K-corrected ratio of the 4.85 GHz radio flux to the optical flux at 4400 A.

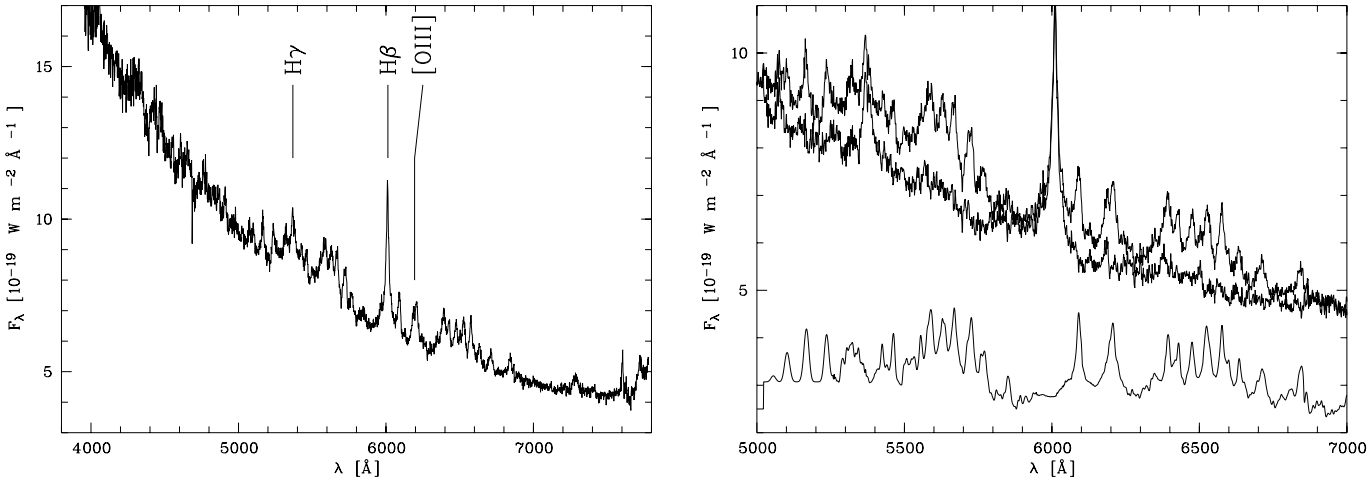

Fig. 12. Optical spectrum of RX J0134.2–4258. The left panel shows the whole wavelength range in which the object was observed, and the right panel displays the FeII subtracted spectrum. The upper spectrum is the original one, the middle one the FeII subtracted spectrum, the lower one is the FeII template used, shown with an offset.

upper limits at 12, 25, and 100 μm (Grupe et al. 1998a). The ROSAT X-ray data in the plot are displayed as the black body plus power law model fit to the RASS and pointed observation spectra. For both cases, the radiation temperature and the hard X-ray spectral slope were fixed (see Table 2).

We used the nonsimultaneous HST (2000) and X-ray spectra to compute α_{ox}, defined to be the point-to-point slope between 2500Å and 2 keV (Wilkes et al. 1994). The pointed ROSAT observation, the ASCA observation and the RASS observation yielded values of α_{ox} of 1.47, 1.68, and 2.00 respectively. Based on the regressions obtained by Wilkes et al. (1994), the predicted values of α_{ox} are 1.61 and 1.43 for radio-quiet and radio-loud AGN of this optical luminosity, respectively. The values obtained for RX J0134.2–4258 lie between these predicted indices, and in two cases are lower than the radio-quiet index. Therefore, although it is impossible to account for the effect of variability, the X-ray emission in RX J0134.2–4258 does not appear to be as strong as is found in other radio-loud AGN with similar optical luminosities.

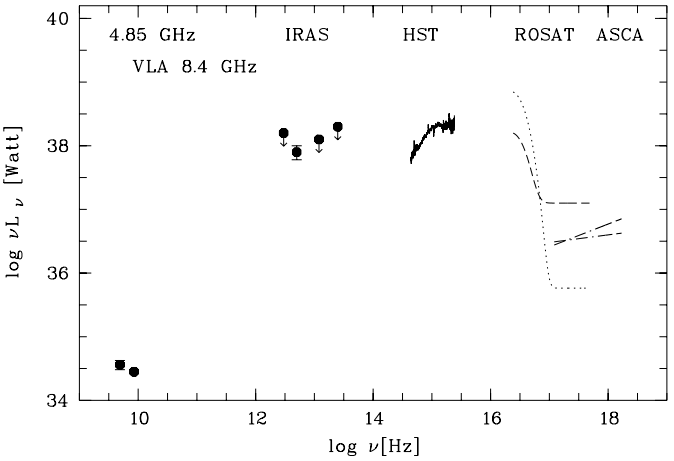

Fig. 13. Spectral Energy Distribution of RX J0134.2–4258. The 4.85 GHz radio point was taken from Wright et al. (1994), IRAS data from Grupe et al. (1998a), and the optical/UV spectrum is from the HST data from Goodrich (2000). The dotted line represents a black body plus power law spectrum of the RASS observation and the dashed line the same for the pointed observation. The ASCA observation is represented by the dashed-dotted line. All points are given in the observers frame.

4. Discussion

4.1. Flux transient behaviour in ROSAT observations

RX J0134.2–4258 was one of the softest AGN at the time of the RASS, but turned into an object with a rather flat X-ray spectrum by the time of its pointed observation. Its behaviour is different from that observed from other 'transient' X-ray AGN. WPVS007 was practically 'off' in all follow-up ROSAT observations after the RASS. We explained this behaviour as a dramatic change in the comptonization parameters that shifted the Big Blue Bump emission out of the ROSAT PSPC range (Grupe et al. 1995b). In IC 3599 (and also NGC 5905) we observed a fading of the X-ray flux over several years. We (Grupe et al. 1995a, but see also Brandt at al. 1995; Bade et al 1996; Komossa & Bade 1999) came to the conclusion that these were X-ray outbursts that could have been caused by tidal disruption of a star by a central black hole.

RXJ0134.2–4258 can be considered to be a 'transient' X-ray source as well. During the RASS, it was practically off at energies above $\sim$ 0.5 keV. While we usually find transient sources that were bright during the RASS, such as WPVS007 or IC 3599, RX J0134–4258 is an exception in that it became bright in its hard X-ray band after the RASS. What makes RX J0134.2–4258 so unusual is its dramatic spectral variability, both on long time scales (between the RASS and pointed observation) and on short time scales (during the pointed observation).

4.2. Precedents for similar behaviour

The results from our study of RX J0134.2–4258 are sufficiently unusual that we have searched the literature for examples of similar behaviour from other objects.

The short term spectral variability observed in RX J0134.2–4258 has some precedent. A hardness ratio analysis of the ROSAT lightcurves from Mrk 766 revealed that the spectrum also hardens when the flux increases. Leighly et al. (1996) first demonstrated that this behaviour was consistent with a non-varying soft excess component plus a power law with varying normalization. Those data have been recently re-examined, and the same results were found (Page et al. 2000).

The long term spectral variability may also have some precedents. Bedford et al. (1988) report the discovery and followup EXOSAT observations of the Seyfert 1.5 galaxy EXO 1128+691. They found the object clearly detected in the EXOSAT LE detector, which is sensitive to soft photons in the 0.05–2.0 keV band, but not detected by the ME detector (0.7–10 keV). The LE detector has no intrinsic energy resolution, but information from exposures using several filters show that the spectrum was very soft, with effective photon index $\Gamma \sim 5$. In contrast, a recent ASCA observation of EXO 1128+691 showed a strong detection in 2–10 keV X-rays (Leighly et al., in preparation). The spectral parameters from the ASCA observation predict 0.4 counts/s in the EXOSAT ME. While this count rate would be somewhat low for detailed spectral analysis (e.g. Turner & Pounds 1989), it should at least have been detected. Therefore, EXO 1128+691 may have undergone a similar spectral transition as experienced by RX J0134.2–4258. A difference is that during the EXOSAT observation, the LE flux was strongly variable, by a factor of 3 on time scales as short as 15 minutes; in contrast, during the pointed ROSAT observation of RX J0134.2–4258 we find that the soft component is constant, and the normalization of the hard component varies.

Another example of a possibly similar spectral transition is the one recently seen in the Narrow-line Seyfert 1 galaxy NGC 4051 (Guainazzi et al. 1998). A BeppoSAX observation of this object found the 2–10 keV flux to be a factor of 20 lower than the historic average. The remaining hard X-ray spectrum was very flat with a strong iron line, suggesting a Compton-reflection dominated spectrum, as is found in Compton-thick Seyfert 2 galaxies. Guainazzi et al. (1998) report that the soft X-ray spectrum was steep, but defer the details to another paper. While this also appears somewhat similar to the case of RX J0134.2–4258, a difference is that while the soft X-ray component is reported to be relatively strong compared with the rest of the spectrum, the *EUVE* light curve shows that it is much weaker than has been seen in previous observations by *EUVE* (J. Halpern 1999, P. comm.).

4.3. Possible origins of the spectral variability

4.3.1. Spectral variability as a change in the warm absorber

Komossa & Fink (1997) and Komossa & Meerschweinchen (2000) investigate whether the spectral variability in RX J0134.2–4258 can be explained by a 'warm' ionized absorber. They noted that there is a deviation in the residuals of a power law fit to the pointed observation near 0.6keV (see Fig. 3) that could be interpreted as an absorption edge from OVII in the rest frame. In contrast, we found that a single power law model does not give a good fit and the spectrum is much better described using two component models in which case the residual disappears. This underlines the fact that with the spectral signal to noise and the low resolution of the PSPC data, a two component model and a warm absorber model cannot be distinguished. The warm absorber requires a very large column density ($10^{23}\mathrm{cm}^{-2}$) to explain the ultrasoft spectrum, and we cannot accommodate such heavy absorption in the ASCA spectra. Furthermore, we do not see a signature of this material in other wavebands. For example, Reynolds (1997) found that warm absorbers are generally associated with optical reddening in a sample of ASCA observations of Seyfert 1 galaxies; in contrast, RX J0134.2–4258 has one of the bluest optical spectra observed in the soft X-ray selected AGN sample. Furthermore, we find that for reasonable parameters, the cloud scenario cannot explain the rather similar spectral variability observed during the pointed observation, simply because for plausible source sizes and cloud velocities, the time scale of variability required is rather longer than observed.

4.3.2. Spectral variability as absence and recovery of a corona

One possible scenario to explain the longterm spectral variability observed in RX J0134.2–4258 is the absence followed by the recovery of the accretion disk corona. A corona is necessary to produce the hard X-rays if the accretion disk is optically thick and geometrically thin. A popular version of the disk-corona model holds that the accretion power is dissipated primarily in the corona, and the disk merely reprocesses part of it (Haardt & Maraschi 1993; Svensson & Zdziarski 1994). However, it has recently been shown that in some Narrow-line Seyfert 1 galaxies, there is far too much power in the soft excess component, believed to be emitted from the disk, to be driven by reprocessing of the hard X-ray component (e.g. Pounds et al. 1995). Thus, the disk emission must be primary, the corona will not be necessary as the primary agent for dissipation of the accretion energy, and therefore it could conceivably be absent. It is possible that RX J0134.2–4258 had no corona during the RASS observation, and it developed one before the pointed observation. The corona regeneration time scale must be fairly short for this scenario to be viable. If the corona is produced by reconnection of buoyant magnetic flux tubes that have been built up to equipartition by convective dynamos in the disk, the relevant time scales are the convection time scales plus reconnection time scales (e.g. Haardt et al. 1994). These authors find a loop variability time scale could be as short as minutes for a $10^6 M_\odot$ object and therefore the corona could conceivably regenerate within the time between the RASS and pointed ROSAT observations. The question of what could cause an object to lose or regrow a corona is a very interesting one that we will not speculate on. On the other hand, it is not necessarily clear that this mechanism could explain the spectral variability observed on short time scales during the pointed observation.

4.3.3. Spectral variability as a strengthening of the radio component

Another possible explanation for the spectral variability observed in RX J0134.2–4258 is suggested by the fact that it is radio-loud, and possibly variable, and the fact that during the ASCA observation the photon index was flat. Radio-loud quasars are well known to have flatter X-ray spectral indices than radio-quiet ones, and they are also known to be brighter X-ray sources (e.g. Lawson & Turner 1997). A widely accepted explanation for this fact is that the X-ray emission includes a additional harder component associated with the radio jet. Therefore, it is possible that the increase in the normalization of the hard X-ray component is caused by a strengthening of the radio jet component. We note that compared with the GINGA sample of quasars, RX J0134.2–4258 is about a factor of 10 deficient in X-ray luminosity (see Lawson & Turner 1997, their Fig. 8). However, taking into account the scatter in the correlation and variability, it is not completely implausible that the hard X-rays are being dominated by a component associated with a radio jet.

This scenario may have a precedent in the case of 3C 273. A set of ASCA observations of this object reveal that a soft excess and iron line appears, and the spectrum becomes steeper when it is fainter (Cappi et al. 1998). It was proposed by Cappi et al. (1998) and also by Haardt et al. (1998) that 3C 273 in its bright X-ray state is dominated by the jet component, and in its faint state, the Seyfert nucleus is revealed. On the other hand, it must be noted that ASCA observations of the other two radio-loud NLS1s revealed canonical NLS1s spectra, i.e. a steep hard X-ray spectrum and a weak soft excess (Siebert et al. 1999; Leighly 1999a).

The existence of radio-loud NLS1s may be somewhat surprising, given the results of Ulvestad et al. (1995) on their small sample of Seyferts, but also because NLS1s, and especially RX J0134.2–4258, are known to be strong emitters of Fe II emission. It has long been considered that Fe II emission is generally weak in radio-loud objects, and [O III] is correspondingly strong. Boroson & Green (1992) in their study of PG quasars found that one of the clearest differences between radio-loud and radio-quiet objects is in their Fe II emission, although steep radio spectrum objects may have strong Fe II (also Joly 1991; Bergeron & Kunth 1984). However, the situation could be similar to that for broad-absorption line quasars (BALQSOs). Early on it was found that BALQSOs are almost never radio-loud (Stocke et al. 1992). Later it was found that many BALQSOs can be described as radio-moderate; they tend to lie at the upper edge of the R distribution for radio quiet quasars (Francis et al. 1993). More recently it has been proposed that radio-moderate or radio-intermediate objects are ones that are in fact not radio-loud but rather have enhanced radio emission because they have a weak radio jet which is beamed in our direction (Falcke et al. 1996). Such an interpretation may be attractive for some NLS1s because of their observed rapid and possibly coherent X-ray variability. However, NLS1s do not appear to be universally radio-intermediate. RX J0134.2–4258 is drawn from a soft X-ray selected sample of AGN (e.g. Grupe 1996; Grupe et al. 1999). A search of the NRAO VLA Sky Survey (NVSS; Condon et al. 1998) reveals that most of the northern ones are very weak radio emitters.

5. Summary and conclusions

We have presented the results of our ROSAT, ASCA and optical observations of the enigmatic soft X-ray AGN RX J0134.2–4258. We found:

- RX J0134.2–4258 has shown a dramatic change in its ROSAT PSPC spectra between its RASS and a pointed PSPC observation made two years later.
- Optically, RX J0134.2–4258 is a Narrow-Line Seyfert 1 galaxy with very strong FeII emission, extremely weak emission from the NLR and with a very blue optical continuum.
- The slopes of the hard component of the ROSAT spectra and the ASCA spectra are consistent, and the ASCA slope is notably flat compared with other NLS1s.
- It is the normalization of the hard X-ray component that varies the most and is primarily responsible for the dramatic spectral change.
- RX J0134.2–4258 has been found to be one of the few NLS1s that are radio loud, and currently holds the record for radio-to-optical flux ratio in NLS1s.
- Physical reasons for the strange spectral behaviour might be a variable warm absorber, the loss and regrowth of a corona above the accretion disk, or an increase in flux from a component associated with a possible jet as indicated by the radio-loudness of this source.

One important problem that applies to most transient AGN is that it is difficult to monitor their behaviour. Often years lapsed between RASS and later pointed observations. Hopefully, in the future with new survey missions it will be easier and faster to discover transients. Then they could be monitored using next-generation all sky monitor experiments such as the approved mission MAXI which will be mounted on the Japanese Experimental Module of the International Space Station, or the proposed Lobster-Eye satellite.

Acknowledgements. We would like to thank Drs. Beverley & Derek Wills and Stefanie Komossa for useful and intensive discussions. We thank Dr. S. Komossa for giving us a preprint of her paper about NGC 5905 and her recent preprint on RX J0134.2–4258. Also we thank Drs. Thomas Boller, Joachim Siebert, Jules Halpern and our referee for their comments and suggestions on the manuscript. We wish to thank Barry Clark and the NRAO staff for granting us 1 hour of engineering time on short notice to obtain the new radio observations which confirmed the association of the PMN radio source with RX J0134.2–4258. This research has made use of the NASA/IPAC Extragalactic Database (NED) which is operated by the Jet Propulsion Laboratory, Caltech, under contract with the National Aeronautics and Space Administration. Also we used the IRAS data request of the Infrared Processing and Analysis Center (IPAC) Caltech. We have made use of the ROSAT Data Archive of the Max-Planck-Institut für Extraterrestrische Physik (MPE) at Garching, Germany. KML gratefully acknowledges

support through NAG5-7971 (NASA LTSA). SALM acknowledges partial support by the Department of Energy at the Lawrence Livermore National Laboratory under contract W-7405-ENG-48 and from the NSF (grant AST-98-02791). The ROSAT project is supported by the Bundesministerium für Bildung und Forschung (BMBF/DLR) and the Max-Planck-Society (MPG).

This paper can be retrieved via WWW from our pre-print server: http://www.xray.mpe.mpg.de/ dgrupe/research/dgrupe.html

References

Bade N., Komossa S., Dahlem M., 1996, A&A 309, L35
Bedford D.K., Vilhu O., Petrov P., 1988, MNRAS 234, 319
Bergeron J., Kunth D., 1984, MNRAS 207, 263
Beuermann K., Thomas H.-C., Reinsch K., et al., 1999, A&A 347, 47
Boroson T.A., Green R.F., 1992, ApJS 80, 109
Brandt W.N., Pounds K.A., Fink H.H., 1995, MNRAS 273, L47
Cappi M., Matsuoka M., Otani C., Leighly K.M., 1998, PASJ 50, 213
Condon J.J., Cotton W.D., Greisen E.W., et al., 1998, AJ 115, 1693
Dickey J.M., Lockman F.J., 1990, ARA&A 28, 215
Falcke H., Sherwood W., Patnaik A.R., 1996, ApJ 471, 106
Francis P.J., Hooper E.J., Impey C.D., 1993, AJ 106, 417
Goodrich R.W., 2000, Proc. of the WE Heraeus-seminar no. 226, Narrow-Line Seyfert 1 galaxies. Bad Honnef, Germany, in press
Grupe D., 1996, Ph.D. Thesis, Universität Göttingen (available via our pre-print server)
Grupe D., Beuermann K., Mannheim K., et al., 1995a, A&A 299, L5
Grupe D., Beuermann K., Mannheim K., et al., 1995b, A&A 300, L21
Grupe D., Beuermann K., Mannheim K., Thomas H.-C., Fink, H.H., 1998a, A&A 330, 25
Grupe D., Wills B.J., Wills D., Beuermann K., 1998b, A&A 333, 827
Grupe D., Beuermann K., Mannheim K., Thomas H.-C., 1999, A&A 350, 805
Guainazzi M., Nicastro F., Fiore F., et al., 1998, MNRAS 301, L1
Haardt F., Maraschi L., 1993, ApJ 413, 507
Haardt F., Maraschi L., Ghisellini G., 1994, ApJ 432, L95
Haardt F., Fossati G., Garndi P., et al., 1998, A&A 340, 35
Iwasawa K., Fabian A.C., Nandra K., 1999, MNRAS, in press
Joly M., 1991, A&A 242, 49
Kellermann K.I., Sramek R., Schmidt M., Shaffer D.B., Green R., 1989, AJ 98, 1195
Komossa S., Fink H.H., 1997, Accretion Disks - New Aspects. Lecture Notes in Physics 487, 250
Komossa S., Bade N., 1999, A&A 343, 775
Komossa S., Meerschweinchen J., 2000, A&A 354, 411
Lawson A.J., Turner M.J.L., 1997, MNRAS 288, 920
Leighly K.M., Mushotzky R.F., Yaqoob T., Kunieda H., Edelson, R., 1996, ApJ 469, 147
Leighly K.M., 1999a, ApJS 125, 297
Leighly K.M., 1999b, ApJS 125, 317
Mannheim K., Grupe D., Beuermann K., Thomas H.-C., Fink H.H., 1996, MPE Report 263, Röntgenstrahlung from the Universe. p. 471
Miller P., Rawlings S., Saunders R., 1993, MNRAS 263, 425
Nandra K., George I.M., Mushotzky R.F., Turner T.J., Yaqoob T., 1997, ApJ 476, 70
Page M.J., Carrera F.J., Mittaz J.P.D., Mason K.O., 2000, MNRAS in press
Pfeffermann E., Briel U.G., Hippmann H., et al., 1986, SPIE 733, 519
Pounds K.A., Done C., Osborne J., 1995, MNRAS 277, L5
Remillard R.A., Grossan B., Bradt H.V., Ohashi T., Hayashida K., 1991, Nat 350, 589
Reynolds C.S., 1997, MNRAS 286, 513
Siebert J., Leighly K.M., Laurent-Muehleisen S.A., et al., 1999, A&A 348, 678
Stocke J.T., Morris S.L., Weymann R.J., Foltz C.B., 1992, ApJ 396, 487
Svensson R., Zdziarski A.A., 1994, ApJ 436, 599
Tanaka Y., Inoune H., Holt S.S., 1994, PASJ 46, L37
Thomas H.-C., Beuermann K., Reinsch K., et al., 1998, A&A 335, 467
Trümper J., 1983, Adv. Space Res. 4, 241
Turner T.J., Pounds K.A., 1989, MNRAS 240, 833
Ulvestad J.S., Antonucci R.R.J., Goodrich W., 1995, AJ 109, 81
Voges W., 1993, Adv. Space. Res. 13, 391
Voges W., Aschenbach B., Boller Th., et al., 1999, A&A 349, 389
Wilkes B.J., Tananbaum H., Worrall D.M., et al., 1994, ApJS 92, 53
Wright A.E., Griffith M.R., Burke B.F., Ekers R.D., 1994, ApJS 91, 111
Zimmermann H.U., Boese G., Becker W., et al., 1998, EXSAS User's Guide, MPE Report